ACS Catalysis

Research Article

pubs.acs.org/acscatalysis

Carbonization of Ethylenediamine Coimpregnated CoMo/Al_2O_3 Catalysts Sulfided by Organic Sulfiding Agent

Hui Ge,*[,†] Xiao-Dong Wen,*[,†,‡] Manuel A Ramos,[§] Russell R. Chianelli,[§] Shanmin Wang,[∥] Jianguo Wang,[†] Zhangfeng Qin,[†] Zhanjun Lyu,[†] and Xuekuan Li*[,†]

[†]State Key Laboratory of Coal Conversion, Institute of Coal Chemistry, Chinese Academy of Sciences, P.O. Box 165, Taiyuan, Shanxi 030001, P. R. China

[‡]Synfuels China, Beijing, 100195 P. R. China

[§]Materials Research and Technology Institute, UT-El Paso, El Paso, Texas 79902, United States

[∥]HiPSEC & Department of Physics, University of Nevada Las Vegas, Las Vegas, Nevada 89154, United States

Supporting Information

ABSTRACT: Coimpregnating binary cobalt/molybdenum/alumina (CoMo/Al_2O_3) catalyst with adding ethylenediamine was studied for carbonization, sulfidation, and hydrodesulfurization using experimental methods. In order to understand the mechanism of carburization of active phases, theoretical CoMo/Carbon models were produced using density functional theory (DFT) method. The results from carbonization of the organic component indicate that the formation of support-like carbon species provokes dispersion of active particles and reduces interaction with support at the active sites (Co, Mo), thus enhancing the HDS activity. Theoretical results from DFT show that carbide-like Co−Mo−C structures are more stable, which can be formed by a simultaneous carburization and sulfidation at an unsaturated S or Mo edge of a (Co)MoS_x slab with CH_3SSCH_3 as both carbon and sulfur source.

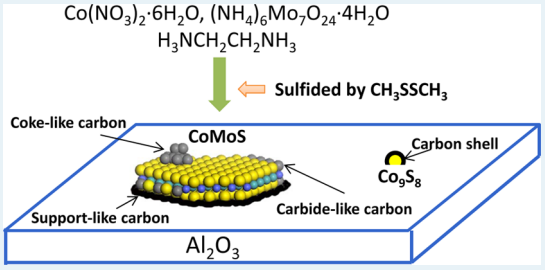

KEYWORDS: *carbonization, hydrodesulfurization, molybdenum, cobalt, ethylenediamine*

1. INTRODUCTION

The hydrotreating process is a key step in upgrading oils derived from petroleum, biomass, or coal, where a CoMo or NiMo catalyst is usually used to achieve the reduction of heterogeneous atoms (S, O, N).[1,2] The term "Co−Mo−S" was coined almost 30 years ago, when observing this phase by means of Mössbauer spectroscopy;[3] later several theoretical models including "decoration",[4] "rim-edge",[5] and recently "Interface"[6] have been produced in order to describe the catalytic mechanism and structural aspects of this particular catalytic phase. In 1986 Hallie et al. reported an enhancement of hydrodesulfurization (HDS) activity using dimethyl disulfide (DMDS) instead of H_2/H_2S as a sulfiding agent during gas/oil catalytic reaction,[7] which was attributed to formation of carbide-like structures at the edge of the active phase.[8] The analysis on stabilized catalyst (after HDS) has detected that a new "carbide" phase can be present in between CoMoS.[9] It was also found that the cobalt can substantially facilitate the carbon replacement of sulfur atoms at the edges of MoS_2 layers when comparing Co-promoted and unpromoted MoS_2 treated with dimethyl sulfide (DMS).[10] The investigation with density functional theory (DFT) showed that replacement of sulfur atom with carbon atom at the edges of MoS_x clusters is energetically favorable.[11] However, scanning tunneling microscopy (STM) combined with DFT research suggested that incorporation of carbon in MoS_2-based catalysts as carbide type phase is not favorable when synthesized with or exposed to DMDS or DMS.[12] Furthermore, Yamada and his colleagues[13,14] found that CoMo/Al_2O_3 catalyst by DMDS activation results in a lower final HDS activity to dibenzothiophene (DBT) than by H_2S activation, and they have no obvious difference in the HDS of straight-run light gas oil. Texier et al.[15,16] observed no significant difference in HDS of DBT or 4,6-dimethyldibenzothiophene when using organosulfides instead of H_2S as sulfiding agent.

Glasson et al.[17] compared carbon bearing CoMo catalysts with carbon free catalysts for thiophene and crude oil desulfurization. They proposed that the observed positive effect is due to the active particles isolated from each other by carbon deposits thus maintaining a high dispersion. Similar results were found in CoMo catalyst presulfided by alkylpolysulfides and MoS_2 catalyst produced by in situ decomposition of $(R_4N)_2MoS_4$.[18,19] CoMo/Al_2O_3 catalyst with addition of ethylenediamine (EN) and with N_2 heat-treating detected two carbon species: one covering the surface of active phase and another inserting between active particles and alumina, showing opposite effects on the HDS performance.[20] Addition of chelating agents in the catalyst preparation

Received: April 10, 2014
Revised: June 9, 2014
Published: June 16, 2014

 © 2014 American Chemical Society

is an effective way to improve catalytic activity. Many chelating ligands such as citric acid, glycol, 1,2-cyclohexanediaminetetraacetic acid, nitrilotriacetic acid, ethylenediaminetetraacetic acid, and EN were used for preparing HDS catalysts and showed improved HDS activity with proper contents.[21−24] To avoid the decomposition of chelating agent, catalyst is usually free from calcinations,[25] and the carbonization is expected to be accompanied by sulfidation.[26]

Until now, the issue concerning the carbonation of HDS catalysts is still in debate. For systematically and explicitly elucidating the roles played by carbon species, we designed a research plot. We first identified the carbon species on HDS catalyst, investigated the formation mechanism of each carbon species, and then illustrated the effect of these carbon species on the HDS activity. In this work, experimentally, CoMo catalysts were prepared with adding EN, and then sulfided with organic agents (thiophene and DMDS). We focus our attention on the carbon species. In order to correlate experimental results a series of computer assisted DFT calculations were performed to investigate the carburization of the "Co−Mo−S" active sites at atomic level.

2. EXPERIMENTAL AND COMPUTATIONAL DETAILS

2.1. Catalyst Preparation. The catalysts were prepared by impregnating γ-Al_2O_3 with NH_3 aqueous solution of $Co(NO_3)_2 \cdot 6H_2O$, $(NH_4)_6Mo_7O_{24} \cdot 4H_2O$, and EN, followed by drying at 110 °C for 12 h. The catalysts with the EN/Co molar ratio of 1 and 2 were denoted as CoMo(EN1) and CoMo(EN2) respectively. Comparison catalyst was prepared by calcining CoMo(EN1) under air at 450 °C for 4 h to remove EN; it was represented as CoMo. The loadings of CoO and MoO_3 for all catalysts (after calcinations) were 3.2 and 16 wt %, respectively.

2.2. Catalyst Sulfidation and HDS Test. The sulfidation and HDS tests were carried out in a fixed bed tubular flow reactor with an inner diameter of 6 mm. The catalysts were ground and sieved to 40−60 mesh before use. In each run, about 0.6 mL of catalyst containing 1.112 mmol of MoO_3 and 0.427 mmol of CoO was loaded. The quartz cloth and quartz sand were filled at the two ends of the reactor tube to keep the catalyst at the center range of the heater. The system was pressured to 1.0 MPa, and then it was heated to 200 °C within 1 h in a hydrogen flow (32 mL/min). As for thiophene sulfidation, thiophene dissolved in *n*-nonane (8.53×10^{-3} mol/mL) was introduced at the velocity of 0.16 mL/min as sulfiding agent. The reactor was kept at 200 °C for 1 h, then raised to 300 °C in 0.5 h, and then kept at the temperature for at least 18 h. After sulfidation, the reactor was cooled down to 240 °C for thiophene HDS test. As for DMDS sulfidation, 1.0 wt % DMDS dissolved in *n*-nonane (0.16 mL/min) was pumped into the reaction system at 200 °C. The reactor was maintained at 200 °C for 2 h, followed by heating to 290 °C in 1 h, and held at this temperature for 4 h; after that, it was raised to 320 °C in 0.5 h, maintained at the temperature for 2 h, and then cooled down to 240 °C. At this temperature, the liquid feed was switched to thiophene solution (8.53×10^{-3} mol/mL). The flow rate was adjusted to keep the conversion of thiophene under 25%. The thiophene content was measured with a Shimadzu GC-14B chromatograph equipped with a FID detector. Before sampling, the catalyst was stabilized for at least 9 h. After reaction, the spent catalyst was purged with *n*-hexane three times, then dried under Ar, and sealed in a glass bottle for characterizations.

Activity at steady-state conditions is described in terms of quasi-turnover frequency (QTOF) using a specific reaction rate according to eq 1:[27]

$$r = (XF)/m \tag{1}$$

The r is the specific rate (mol molCo $^{-1}$ s^{-1}), X is the conversion of thiophene, F is the molar flow rate of this reactant (mol s^{-1}), and m refers to the mole number of Co metal, based on the postulation that the active site is "Co−Mo−S" structure.[28]

2.3. Catalyst Characterization. The sulfur content in spent catalysts was determined by a microcoulometer (KZDL-3, Hebi-gaoke, China) using the coulometry titration method.[29] The carbon elemental analysis was obtained through combustion of sample and quantitative evaluation of CO_2.[30]

Temperature-programmed oxidation (TPO) was conducted in a TP-5000 (Tianjing-Xianquan, China) quartz microreactor. About 40 mg of spent catalyst was pretreated under Ar at 150 °C for 2 h and then cooled down to room temperature. The gas was switched to a mixture of 5% O_2−95% Ar (30 mL/min), and then the system was heated from room temperature up to 700 °C at 10 °C/min and held at that temperature for 30 min. CO, CO_2, H_2O, and O_2 in effluent were measured by a quadrupole mass spectrometer (OmniStar 200).

Temperature-programmed reduction of sulfided catalysts (TPR-S) was carried out on the same instrument used for TPO. About 40 mg of catalyst was flushed for 2 h with Ar at room temperature. Then the gas flow was switched to hydrogen (30 mL/min), and profiles began to be recorded. After stabilization, the system was heated from room temperature up to 700 °C at a rate of 10 °C/min and kept at this temperature for 30 min. The signals of H_2 and organic effluents were recorded by an OmniStar 200 mass spectrometer.

Ultraviolet−visible diffuse reflectance spectroscopy (DRS) was conducted on a Varian Cary300 UV−vis spectrophotometer from 200 to 800 nm.

High-resolution transmission electron microscopy (HRTEM) analysis for spent catalysts was performed on a JEOL JEM-2010 microscope operated at 200 kV. For estimation of the stacking and size distribution of Co/MoS_2 crystallites, more than 400 crystallites were measured for each sample. The average slab length and stacking number were calculated according to eq 2:

$$\bar{M} = \frac{\sum_{i=1}^{n} n_i M_i}{\sum_{i=1}^{n} n_i} \tag{2}$$

M_i is the slab length or stacking number of a Co/MoS_2 unit, and n_i is the number of Co/MoS_2 particles whose slab size or stacking number falls in a determined range or number.

2.4. Model and Method of DFT Calculation. *2.4.1. Surface Model.* A periodic slab model was used to depict the surface of Co−Mo−S or MoS_2. Figure 1 shows the Co-promoted MoS_2 model

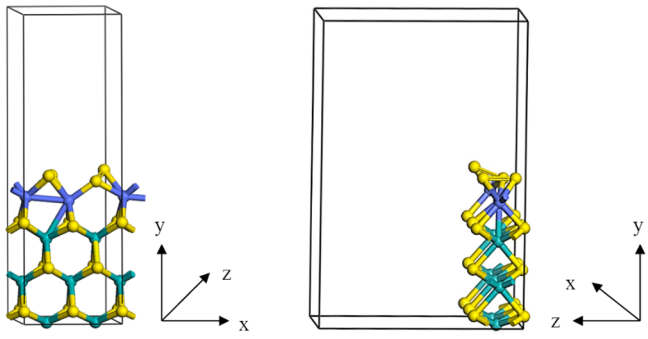

Figure 1. $Co-Mo_8S_{16}$ models. Each model comprises one cobalt row and three molybdenum rows. Green balls, molybdenum atoms; purple balls, cobalt; yellow balls, sulfur.

including one S−Co−S row (top) and three S−Mo−S rows (below) in the y direction, two units in the x direction, and one layer in the z direction. To verify the reliability of the models, a series of calculations using different sizes of Co-promoted MoS_2 models were performed by varying the periodicity in the x direction (two and four), the number of rows in the y direction (four to eight), and the number of layers in the z direction (one and two). The different models led to a similar change (≤0.06 eV) in relative energy (ΔE). Therefore, the single-layer four-row ($2 \times 4 \times 1$) model was used to study the carburization and

dx.doi.org/10.1021/cs500477x | ACS Catal. 2014, 4, 2556−2565

sulfidation of Co/MoS_2 slab so as to accelerate the convergence of DFT calculation.

2.4.2. Method. DFT calculations were performed using the DMol^3 module in Material Studio (version 4.4). The electronic wave functions are expanded in numerical atomic basis sets defined on an atomic-centered spherical-polar mesh. The doubled numerical basis set plus *d* functions (DND) is used for all elements except for transitive metals, which are approximated by the effective core potential (ECP). Spin unrestricted is included for open shell structures. The exchange-correlation energy is approximated by the Becke exchange functional in conjunction with the Perdew–Wang correlation functional (GGA-BP). The medium quality mesh size is used for the numerical integration. The tolerances of energy, gradient, and displacement convergence are 0.00002 Ha, 0.004 Ha/Å, and 0.005 Å, respectively. The real space cutoff of atomic orbitals is set to 4.5 Å, allowing for efficient calculations without loss of accuracy. The Kohn–Sham equations are solved by a SCF (self-consistent field) procedure. The Fermi smearing of 0.0005 is used to count the orbital occupancy, and *k*-point set of (2 × 1 × 3) is applied to all calculations. The atoms in the bottom two S–Mo–S rows are fixed, and atoms in the top two rows are allowed to relax. All investigated structures are geometrically optimized.

3. RESULTS AND DISCUSSION

3.1. Catalyst Sulfidation by Thiophene. When thiophene was used as sulfiding agent, the sulfidation of metal oxides was accompanied by the desulfurization of thiophene. The sulfidation of metal oxides can be followed by thiophene conversion. As shown in Figure 2, at initial stage, thiophene

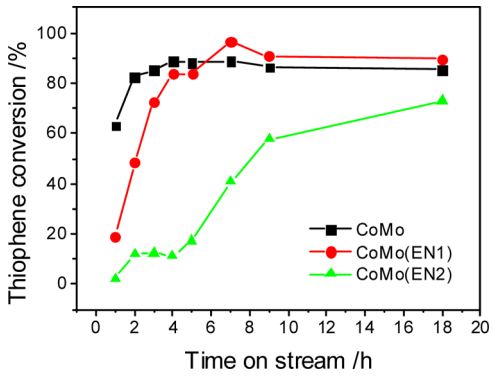

Figure 2. Sulfidation of oxidized catalysts by thiophene. Sulfidation conditions: t = 300 °C, p = 1.0 MPa, LHSV = 16 h^{-1}, $V(H_2)/V(oil) \approx$ 200.

conversion follows a sequence of CoMo > CoMo(EN1) > CoMo(EN2). After about 5 h in stream, CoMo(EN1) surpassed CoMo. But for CoMo(EN2), sulfidation was not fulfilled even at the end of the test.

The thiophene conversion increased with the time on stream, suggesting the formation of Co–Mo–S active sites. As for EN containing catalysts, the conversion increases more slowly, in agreement with the supposition that sulfidation of cobalt is retarded by the cooperation with chelating agent.[31] Owing to the sulfidation of Co^{2+} postponed until the sulfidation of MoO_3 is almost completed, so the cobalt promoters can decorate at the edges of preformed MoS_2, avoiding formation of Co_9S_8, the no active phase.[32] This explains that the CoMo(EN1) catalyst showed higher thiophene conversion than CoMo catalyst after 5 h sulfidation. EN is a bidentate ligand, each Co^{2+} ion was averagely chelated by one and two EN molecules in CoMo(EN1) and CoMo(EN2), respectively. The Co^{2+} ion in CoMo(EN2) coordinated on average by four N atoms, and it become more difficult to be sulfided. Therefore, CoMo(EN2) was not fully sulfided by thiophene at 300 °C even after 18 h on stream.

3.2. Catalyst HDS Tests. The QTOF calculated according to eq 1 are presented in Figure 3. The CoMo(EN1) catalyst

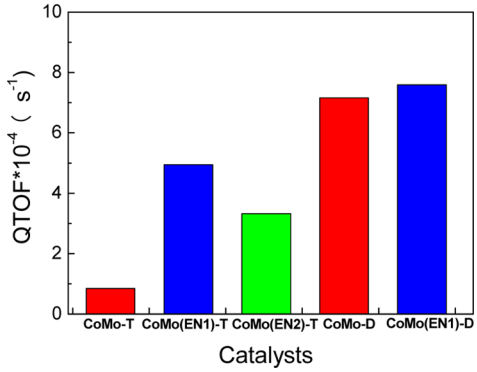

Figure 3. Thiophene HDS activities over sulfided catalysts. Reaction conditions: t = 240 °C, p = 1.0 MPa, $V(H_2)/V(oil) \approx$ 200. Thiophene and DMDS sulfidations are designated -T and -D respectively.

had the highest activity among the three catalysts sulfided with DMDS, and had a better performance in the two catalysts sulfided with thiophene. CoMo catalyst sulfided by DMDS showed a QTOF value 8.5 times as high as for that sulfided by thiophene. Due to the strong interaction with Al_2O_3 support,[28] the Co and Mo oxides in CoMo catalyst are difficult to be sulfided and, thus, are sensitive to sulfiding agent. As for CoMo(EN1) catalyst, the addition of chelating agent reduces the interaction between the active metals and support.[33,34] As a result, the QTOF of DMDS sulfidation is only 1.5 times as high as that of thiophene sulfidation. Owing to cobalt ion cooperating with one EN molecule, its sulfidation is retarded after the formation of MoS_2 phase, so the cobalt ion has more chance to anchor at the edge of preformed MoS_2 crystallites.[32] The efficient formation of Co–Mo–S active phase with DMDS sulfidation makes CoMo(EN1) show the highest HDS activity. However, as for the CoMo(EN2) catalyst sulfided by thiophene, the cobalt ion cooperated with two EN molecules strongly postponed the formation of active Co–Mo–S sites. The HDS activity over this catalyst fell between that of CoMo(EN1) and CoMo. This indicates that the content of EN needs to be appropriately controlled.

3.3. Sulfur and Carbon Contents. Table 1 lists the sulfur and carbon contents in the spent catalysts. For thiophene sulfidation, the CoMo(EN1) catalyst has higher sulfiding degree than the two other catalysts, and CoMo(EN2) exhibits

Table 1. Elemental Analysis of S and C Contents of Spent Catalysts

catalysts	sulfiding agent	S contents (%)	C contents (%)	degree of sulfidation[a] (%)
CoMo	thiophene	5.37	4.91	71
CoMo	DMDS	7.87	1.52	101
CoMo(EN1)	thiophene	7.70	4.84	103
CoMo(EN1)	DMDS	9.21	1.89	119
CoMo(EN2)	thiophene	5.36	4.30	71

[a]100% degree of sulfidation refers to transformation all Mo and Co atoms into MoS_2 and CoS.

dx.doi.org/10.1021/cs500477x | ACS Catal. 2014, 4, 2556–2565

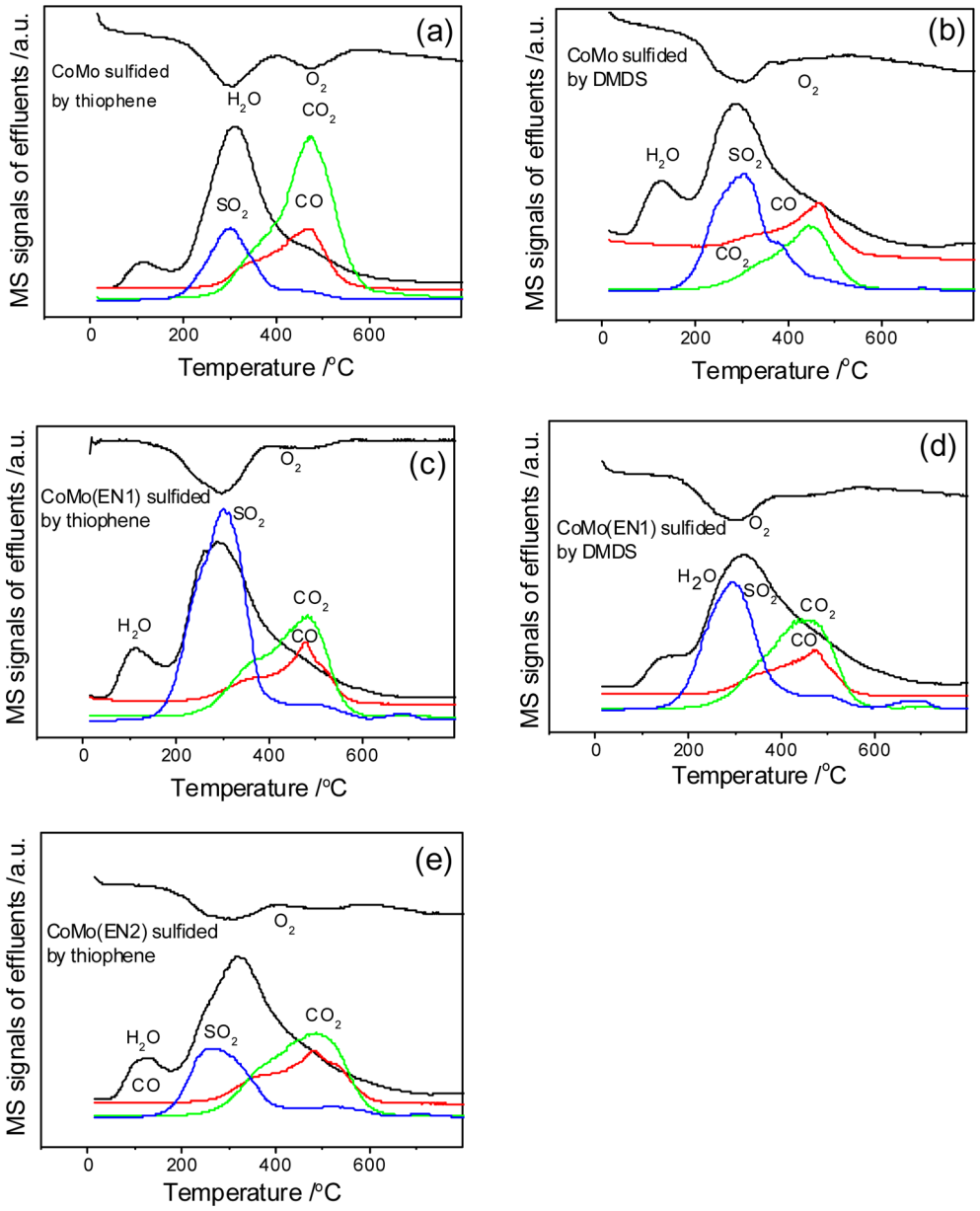

Figure 4. TPO profiles of catalysts sulfided by different sulfiding agents.

similar sulfiding degree to CoMo catalyst. For DMDS sulfidation, a similar trend is obtained. This result suggests that the amount of EN is a key factor to improve the sulfidation. The CoMo(EN1) sulfided by DMDS presented a sulfiding degree of 119%. Our previous DFT calculations suggested that the Mo edge covered by sulfur atoms is thermodynamically favorable.[35] Under sufficiently sulfiding conditions, the Mo edge can also be covered with sulfur atoms, leading to the S/Mo > 2.

The carbon contents fall in the ranges 4−5% and 1−2% for the catalysts sulfided by thiophene and by DMDS, respectively. A large quantity of carbon was deposited on the catalysts with thiophene sulfidation, resulting in a detrimental effect to HDS activity. This suggests that some active particles may be covered by carbon species. However, using carbon element analysis cannot obtain detailed information about the carbon species.

3.4. TPO. Figure 4 shows the TPO profiles of spent catalysts. For CoMo catalyst, the main peak of SO_2 is around 300 °C, and a shoulder peak appears at 450 or 380 °C for thiophene or DMDS sulfidation, respectively. The shoulder peak accompanies with the release of CO and CO_2 for thiophene sulfiding sample. CO and CO_2 main peak is located at around 480 °C, and shoulder peaks occur at lower temperature (about 320−350 °C). The H_2O profile shows the first peak at about 110 °C, afterward evolveing with SO_2.

According to ref 17,23,26,36−38, carbon species on CoMo catalysts can be classified as follows: (1) Carbide-like (Co−Mo−C) species in which carbon atoms located at the active edges of (Co)MoSx slabs. (2) Coke-like species covering active phase or support, which are further differentiated to reactive coke and the refractory coke; the reactive coke containing both sulfur and carbon can be removed more easily during HDS, while the refractory coke containing only carbon is difficult to remove from the catalyst surface. (3) Support-like carbon, which participates in the structure of the active phase as an intermediate support.

Comparing the profile of SO_2 with those of CO or CO_2, the shoulder peaks of CO or CO_2 around 350 °C accompany the

dx.doi.org/10.1021/cs500477x | ACS Catal. 2014, 4, 2556−2565

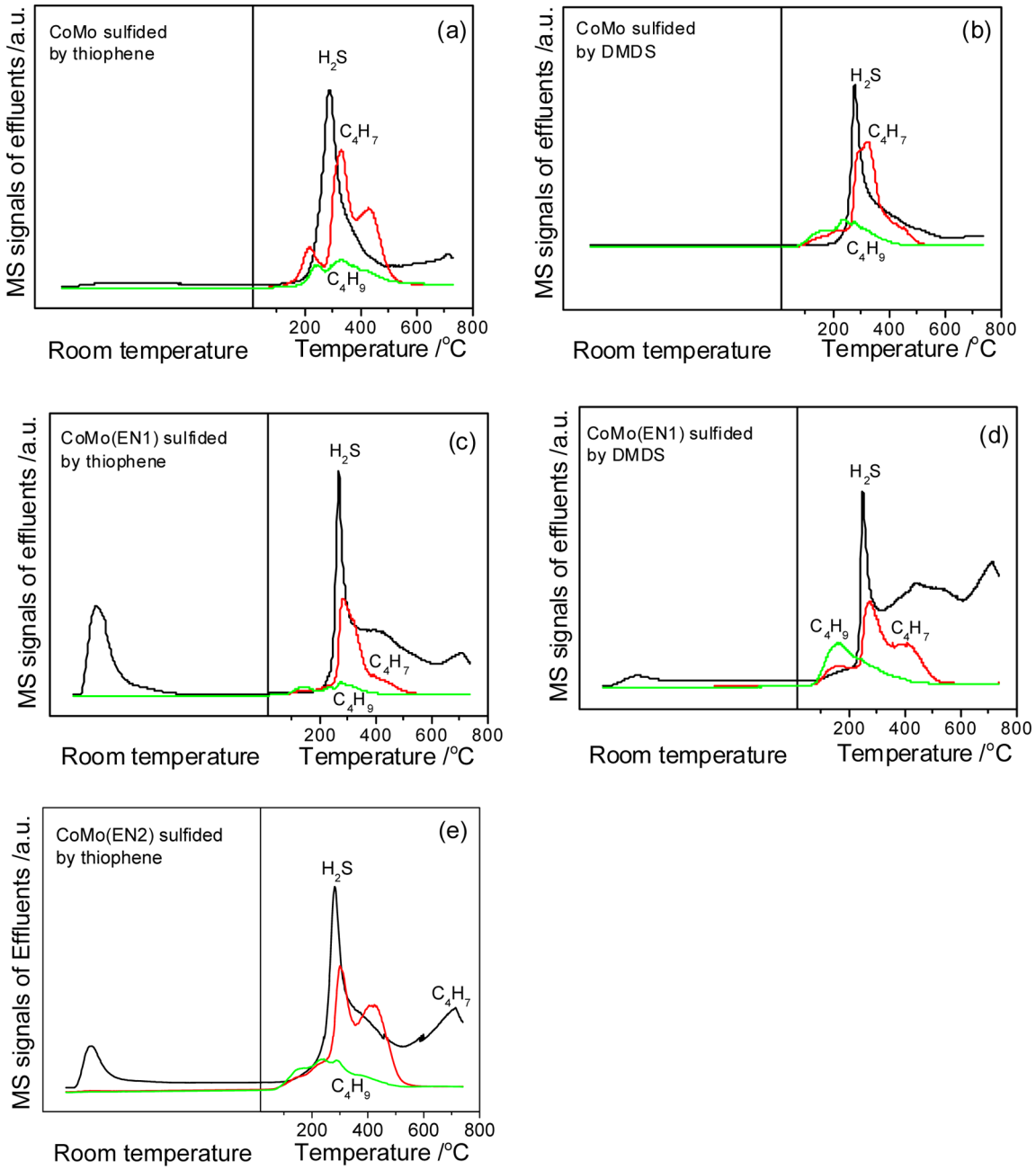

Figure 5. TPR-S profiles of catalysts sulfided by different sulfiding agents.

release of SO_2, which possesses a low percentage in total carbon content. They may be attributed to the reactive coke or carbide-like species. Owing to covering the surface or edge of Co/MoS_2 crystallites, they are oxidized simultaneously with sulfur species. As for support-like carbon species, due to staying between the active metal and support, it needs higher temperature to be burned out; we assign the oxidization of carbon around 450 °C to this carbon species. The refractory coke is mainly found in deactivated catalysts. In our experiment, the opportunity of forming this coke is expected to be low, so we exclude it.

The SO_2 peak around 300 °C is ascribed to the oxidation of $(Co)MoS_x$ phases. For thiophene sulfidation, the SO_2 shoulder peak at about 470 °C is close to the main peaks of CO and CO_2, suggesting that this part of sulfur interacts with support carbon. For DMDS sulfidation, the shoulder peak appear at about 380 °C, ahead of the oxidation of the main CO and CO_2 components; we propose that these sulfur anions may bridge the Mo ions and Al ions in support. The oxidation of sulfur is accompanied with the release of water, indicating that there are hydrogen atoms absorbed on the surface of the Co−Mo−S active phase, in agreement with the prediction of theoretical computations.[39]

For the catalysts with addition of EN, the main peak of SO_2 around 300 °C is assigned to the sulfur atoms bonded directly with active metals. The weak peak at about 500 °C, close to the main peak of CO_2 and CO, can be attributed to sulfur species in the intermediate carbon support. The third sulfur species is oxidized around 690 °C, at which the carbon oxidation has finished. We deduce that some cobalt ions have been sulfided to Co_9S_8 and packed by carbon due to Co^{2+} ions coordinated by EN. This part of Co_9S_8 could be oxidized only after the carbon shell was burned out. Thus, the peak around 690 °C is

dx.doi.org/10.1021/cs500477x | ACS Catal. 2014, 4, 2556−2565

assigned to the oxidation of Co_9S_8 packed by carbon shell. This peak does not appear in CoMo catalyst, suggesting that this sulfur species is related to EN.

The carbon oxidation of catalysts added with EN is similar to that of CoMo catalyst. The main peak of CO_2 and CO at about 480 °C represents support-like carbon species, which may contain sulfur. The shoulder peaks at about 350 °C correspond to the oxidation of carbide-like carbon or coke-like carbon. The water peak at about 110 °C is attributed to the absorbed water; at higher temperature, the water signal following the evolution of SO_2, CO_2, and CO can be ascribed to the oxidation of hydrogen in the Co−Mo−S active phase and carbon species.

3.5. TPR-S. The TPR-S was carried out to investigate the situation of sulfidation and carbonization of catalysts. Figure 5 shows the profiles of H_2S and hydrocarbons (represented by the MS signals of $C_4H_7^+$ and $C_4H_9^+$) in effluents. For the CoMo catalysts sulfided by thiophene or DMDS, a H_2S peak with a tail appears around 280 °C. The main peak corresponds to the SO_2 main peak in TPO, attributed to the reduction of sulfur in CoMoS structures.[40] The tail corresponds to the shoulder peak of SO_2 in TPO, involved in the reduction of sulfur species interacting with the support-like carbon or alumina.

The mass signals of $C_4H_7^+$ and $C_4H_9^+$ fragments are used to detect the reduction of carbon species. The CoMo catalyst with thiophene sulfidation shows obvious signal of $C_4H_7^+$ over 400 °C, in contrast with DMDS sulfidation. This is consistent with the results of chemical analysis of carbon content.

For CoMo catalysts with EN addition, a H_2S peak is apparently observed when switching to hydrogen gas at room temperature, suggesting that the sulfur atoms coordinate weakly with Mo or Co cations. At ambient temperature, they are reduced by hydrogen to form coordinately unsaturated sites (CUS), the active sites of desulfurization.[41] Increasing temperature from ambient temperature to 750 °C, three peaks of H_2S appear at about 260, 420, and 700 °C respectively, consistent with the three SO_2 peaks in TPO. The three peaks are ascribed to the reduction of Co−Mo−S phases, sulfur species in intermediate support carbon, and the Co_9S_8 crystals packed by carbon deposits, respectively. For the carbon species, the weak peak observed at low temperature may correspond to the absorbed hydrocarbons. The peak around 290 °C, corresponding to the main peak of H_2S, may be attributed to the carbide-like or coke-like carbon. And the peak around 420 °C may be ascribed to support-like carbon.

The CoMo(EN1) catalyst sulfided by DMDS shows an apparent peak of H_2S at about 420 °C. The temperature corresponds to the reduction of support-like carbon, suggesting that the sulfur species may have some relation with support carbon. The H_2S peak above 700 °C for CoMo(EN1) and CoMo(EN2) can be ascribed to the reduction of Co_9S_8 packed by carbon shell.

From the results of TPO and TPR-S, the coordination of EN to Co ions indeed promotes the formation of Co−Mo−S structures, but the carbonization of EN, on the other hand, inhibits the Co promoters to move to the edge of MoS_2 slabs, leading to the formation of Co_9S_8. They have opposite effects to catalytic activity. Thus, a compromised content of EN is essential for high HDS activity. The carbon species are not only carbon comprised, but also contain sulfur or hydrogen components.

3.6. UV−Vis DRS. The UV−vis DRS profiles of fresh and spent catalysts are presented in Figure 6 and Figure 7

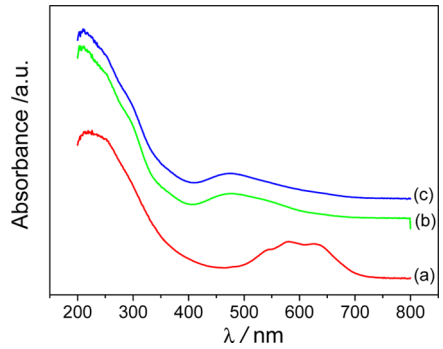

Figure 6. UV−vis DR spectra of oxidized catalysts: (a) CoMo, (b) CoMo(EN1), and (c) CoMo(EN2).

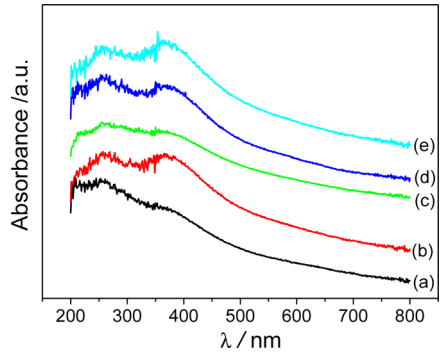

Figure 7. UV−vis DR spectra of sulfided catalysts. Sulfidation by thiophene: (a) CoMo; (b) CoMo(EN1); (c) CoMo(EN2). Sulfidation by DMDS: (d) CoMo; (e) CoMo(EN1).

respectively. For the fresh catalysts, a triplet at about 600 nm is observed in CoMo catalyst, representing no active $CoAl_2O_4$ spinel.[42] With addition of EN, the absorbance of Co^{2+} shifts to about 470 nm. This is consistent with the results of Ni^{2+} coordination with EN in $NiMoEn/SiO_2$ catalyst.[24] The result suggests that the Co^{2+}−EN complexes inhibit the formation of the $CoAl_2O_4$ phase.

For the absorbing range of Mo, the two peaks are observed around 260 and 370 nm, respectively, in spent catalysts (Figure 7). The strongest intensities of absorbance are found over the three catalysts with high sulfiding degrees and catalytic activities, namely, CoMo catalyst sulfided with DMDS and CoMo(EN1) sulfided with DMDS and thiophene. The two catalysts with low sulfiding degrees and catalytic activities, namely, thiophene sulfided CoMo and CoMo(EN2) catalyst, only present weak absorbance at this range. We propose that the strength of the two peaks may be used to qualitatively predict the sulfiding status of Mo active metals, as well as the HDS activities.

3.7. HRTEM. The dispersion and morphology of Co/MoS_2 crystallites in spent catalysts were observed by HRTEM. With this technique it is possible to visualize the typical lattice fringes of the basal planes of Co/MoS_2 structures with ∼6.2 Å interplanar distances (Figure S1 in the Supporting Information). Figure 8 shows the length and stacking number dispersions of Co/MoS_2 crystallites. For all catalysts, about 90% percent of Co/MoS_2 particles fall into the range of 1−3 nm in length. The single layer is dominant, followed by double-layer; multilayer is not over 10%. The CoMo catalyst sulfided by thiophene or DMDS shows higher percentage of single layer stacking, whereas thiophene sulfided CoMo(EN2) presents

dx.doi.org/10.1021/cs500477x | ACS Catal. 2014, 4, 2556−2565

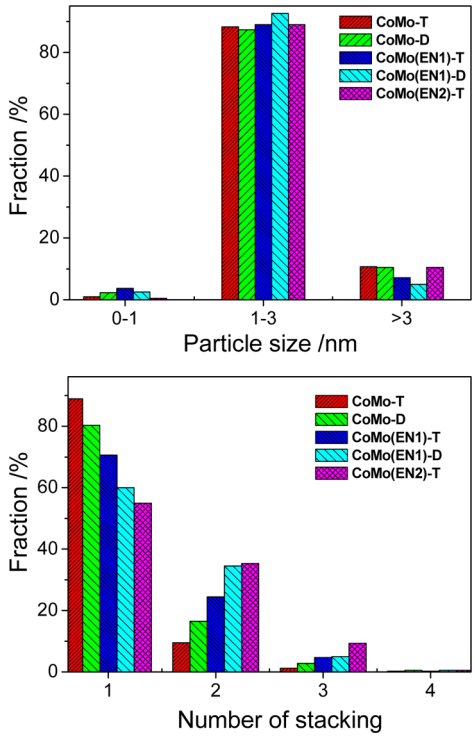

Figure 8. Distribution of slab length and stacking number of $CoMoS_2$ particles in spent catalysts. Thiophene and dimethyl disulfide sulfidations are designated -T and -D respectively.

higher percentage of multilayer stacking. CoMo(EN1) sulfided by Thiophene or DMDS stays in the midway.

Table 2 lists the statistic average length and stacking number of active particles. The average slab lengths of CoMo(EN1)

Table 2. Average Slab Length and Stacking Number of Co/MoS_2 Particles in Spent Catalysts

catalysts	methodology	av slab length (nm)	av stacking no.
CoMo	thiophene	2.13	1.13
CoMo	DMDS	2.02	1.24
CoMo(EN1)	thiophene	1.91	1.35
CoMo(EN1)	DMDS	1.89	1.46
CoMo(EN2)	thiophene	2.13	1.55

catalysts sulfided by thiophene and DMDS are smallest. This can be attributed to the Co(MoS_2) particles being kept small by the isolating effect of support carbon.[17] Ramos et al. observed that the carbon in a TEM Cu/C grid indeed reacts with Co/MoS_2 catalyst.[43] Smaller average length is favorable to enhance the edge area and then increase the number of active sites.

For the thiophene and DMDS sulfided CoMo catalysts, the average stacking number of Co/MoS_2 slabs is 1.13 and 1.24 respectively. After addition of EN, the average stacking number increases to about 1.4 for CoMo(EN1) and 1.55 for CoMo(EN2) respectively, suggesting that the interaction of support with active phase continually decreased with the addition of EN.[44] Extensive research has found that the intrinsic catalytic properties of Co−Mo−S structures can be strongly influenced by the support interaction. Candia et al.[45] observed that increasing the sulfiding temperature from 673 to 873 K resulted in the formation of modified Co−Mo−S structures (termed type II Co−Mo−S) which had a substantially higher intrinsic activity than those formed at the lower temperatures (termed type I Co−Mo−S). The low activity of type I Co−Mo−S is due to the presence of some Mo−O−Al linkages between the MoS_2 and the alumina support. The presence of such species in sulfided catalysts may be related to the strong tendency of Mo interacting with surface alumina OH groups during catalyst preparation.[46−48] The insertion of the carbon species between Mo and alumina decreases the interaction of support with Mo and induces the type I to type II transformation. The high HDS activities over sulfided CoMo-(EN1) can be partly attributed to the higher stacking and smaller size of Co/MoS_2 particles, as well as the proper interaction with support-like carbon species. As for CoMo-(EN2), the decreased support interaction leads to form larger Co/MoS_2 particles, and the HDS activity decreased.

3.8. The DFT Calculation. From the TPO experiments, we found that the carbide-like carbon species, if existing, only take up a low percentage in the total carbon content on sulfided catalyst. Using conventional technologies it is difficult to characterize this carbon species. DFT has proven to be a very powerful tool for the prediction of structural and electronic properties in both chemistry and physics. Thus, the atomic insights on the carbide-like structures are provided through DFT calculations. It has been evidenced by STM observation and DFT calculation that Co−Mo−S structures are easier to form at S edge than at Mo edge.[49] But partly Co substituted Mo edge is thermodynamically favored.[50] Therefore, the carburization process is investigated on the S edge with 100 or 50% Co substitution and on the Mo edge with 50 or 0% Co substitution, respectively. The most important results are reported as follows. Many more results and related discussions are presented in sections B1, B2, and B3 of the Supporting Information.

3.8.1. The Carburization of 100% Surface Mo Atoms Substituted by Co Promoters at the S Edge. In real sulfiding conditions, different carbon species may serve as carburizing sources. Thus, we study the carburization procedure using C, CH, CH_2, CH_3, CH_3S, and CH_3SSCH_3 as carburizing agent. Figure 9 shows the optimized structures of the surface sulfurs replaced by carbon atoms in Co−Mo_8S_x periodic models. Equation 3 shows the reactive process of carburization by CH_y species at the S edge; the sulfur is assumed to release as H_2S; the ΔE is calculated using eq 4. For CH_3S or CH_3SSCH_3, the carburization is illustrated in eq 5, and ΔE is calculated according to eq 6, where m equals 1 or 2, corresponding to CH_3S or CH_3SSCH_3, respectively.

$$\text{Co}-\text{Mo}_8\text{S}_x + n\text{CH}_y = \text{Co}-\text{Mo}_8\text{S}_{x-n}\text{C}_n + n\text{H}_2\text{S} + \left(\frac{1}{2}ny - n\right)\text{H}_2 \quad (3)$$

$$\Delta E = \left[E(\text{Co}-\text{Mo}_8\text{S}_{x-n}\text{C}_n) + nE(\text{H}_2\text{S}) + \left(\frac{1}{2}ny - n\right)E(\text{H}_2)\right] - [E(\text{Co}-\text{Mo}_8\text{S}_x) + nE(\text{CH}_y)] \quad (4)$$

$$\text{Co}-\text{Mo}_8\text{S}_x + n(\text{CH}_3\text{S})_m + \frac{1}{2}nm\text{H}_2 = \text{Co}-\text{Mo}_8\text{S}_{x-nm}\text{C}_{nm} + 2nm\text{H}_2\text{S} \quad (5)$$

dx.doi.org/10.1021/cs500477x | ACS Catal. 2014, 4, 2556−2565

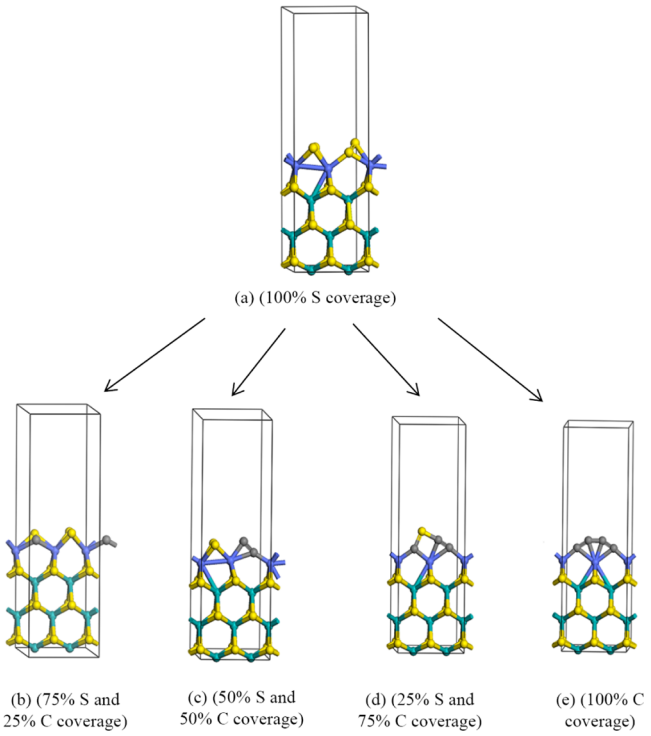

Figure 9. Replacement of sulfur atoms by carbon atoms on the S edge with 100% sulfur coverage and 100% Mo atoms substituted by Co promoters.

$$\Delta E = [E(\text{Co–Mo}_8\text{S}_{x-nm}\text{C}_{nm}) + 2nmE(\text{H}_2\text{S})] - \left[E(\text{Co–Mo}_8\text{S}_x) + nE((\text{CH}_3\text{S})_m) + \frac{1}{2}nmE(\text{H}_2)\right] \quad (6)$$

The ΔE of carburization by different carbon sources is listed in Table 3. When C, CH, or CH_2 is carburizing agent, negative reaction energy is observed, indicating that carburization by C, CH, and CH_2 is thermodynamically favored. The carburization ability is C > CH > CH_2.

When CH_3, CH_3,S or CH_3SSCH_3 is used as carburizing source, the ΔE becomes positive, indicating that energy is needed for carburization. This result is in agreement with the STM observation.[12] For the CH_3 carburization species, the first carbon replacement needs at least 1.06 eV; and the ΔE of the second, the third, and the fourth carbon atom replacement is 0.24, 0.20, and −0.87 eV respectively. As for CH_3S as carburization source, the ΔE of the first, the second, the third, and the fourth carbon atom replacement is 1.21, 0.40, 0.35, and −0.72 eV respectively, indicating that the deep carburizations are more favorable in energy. For CH_3SSCH_3 as carbon source, the ΔE of the first, the second, the third, and the fourth carbon atom substitution becomes 2.58, 1.77, 1.73, and 0.65 eV respectively. The carburization capability is CH_3 > CH_3S > CH_3SSCH_3. It is found that the first carbon replacement is the most difficult step for carburization. With the increase of carbon substitution number, the carburization becomes easier, namely, carburization is facilitated by itself. The replacement of sulfur atom by carbon atom at the S edge is energetically unfavorable when using sulfiding agent CH_3SSCH_3 as carbon source.

Using the model of sulfur atoms replaced by carbon atoms, we investigate the factors which influence the carburization. We observed that the increase of Mo substitution by Co and the increase of sulfur covering will be favorable for the carbon substitution at the S edge. ΔE of sulfur atom replacement by carbon atom at Mo edge is similar to that at the sulfur edge (see the Supporting Information).

3.8.2. The Simultaneous Sulfidation and Carburization at the S and the Mo Edge. As discussed above, the replacement of sulfur atom with the carbon atom in CH_3SSCH_3 molecule is thermodynamically unfavored. So we investigate the simultaneous sulfidation and carburization at unsaturated edge using CH_3S and CH_3SSCH_3 as both carbon and sulfur source. The reactions are expressed by eq 7, and the reaction energies are calculated according to eq 8, where the m equals 1 or 2 for CH_3S or CH_3SSCH_3, respectively. The process is schematized in Figure 10, and the computed reaction energies are listed in Table 4.

$$\text{Co–Mo}_8\text{S}_x\text{C}_y + \frac{1}{m}(\text{CH}_3\text{S})_m = \text{Co–Mo}_8\text{S}_{x+1}\text{C}_{y+1} + \frac{3}{2}\text{H}_2 \quad (7)$$

$$\Delta E = \left[E(\text{Co–Mo}_8\text{S}_{x+1}\text{C}_{y+1}) + \frac{3}{2}E(\text{H}_2)\right] - \left[E(\text{Co–Mo}_8\text{S}_x\text{C}_y) + \frac{1}{m}E((\text{CH}_3\text{S})_m)\right] \quad (8)$$

For the sulfur edge of 100% Mo substituted by Co, simultaneous sulfidation and carburization is influenced by the degree of carburization. When the surface changes from 50% sulfur coverage to 50% carbon coverage, the ΔE changes from 1.53 and 2.88 eV to −1.65 and −0.30 eV for CH_3S and CH_3SSCH_3, respectively. The carburization process takes place from an endothermic one to an exothermic one. At bared Mo edged, the ΔE is −1.02 and 0.31 eV for simultaneous sulfidation and carburization by CH_3S and CH_3SSCH_3, respectively, suggesting that simultaneous sulfidation and carburization can also appear at Mo bared edge.

From the DFT results above, we suggest that with DMDS as sulfiding agent the carburization is not by replacement of sulfur atom with carbon atom in DMDS molecule. The possible process is that the sulfur atom and carbon atom in DMDS molecule simultaneously coordinate on the unsaturated edges of $(\text{Co})\text{MoS}_x(\text{C}_y)$ particle. From the results in Table 4, we

Table 3. Reaction Energy (ΔE, eV) of Carburization on the S Edge with 100% Sulfur Coverage and 100% Surface Mo Atoms Substituted by Co Promoters Using Different Carburization Sources

process[a]	carbon substitution (%)	C	CH	CH_2	CH_3	CH_3S	CH_3SSCH_3
a to b	25	−5.27	−4.03	−2.36	1.06	1.21	2.58
a to c	50	−11.36	−8.87	−6.22	1.30	1.61	4.35
a to d	75	−17.49	−13.76	−8.76	1.50	1.96	6.08
a to e	100	−24.70	−19.73	−13.05	0.63	1.24	6.73

[a]Process is schematized in Figure 9.

dx.doi.org/10.1021/cs500477x | ACS Catal. 2014, 4, 2556−2565

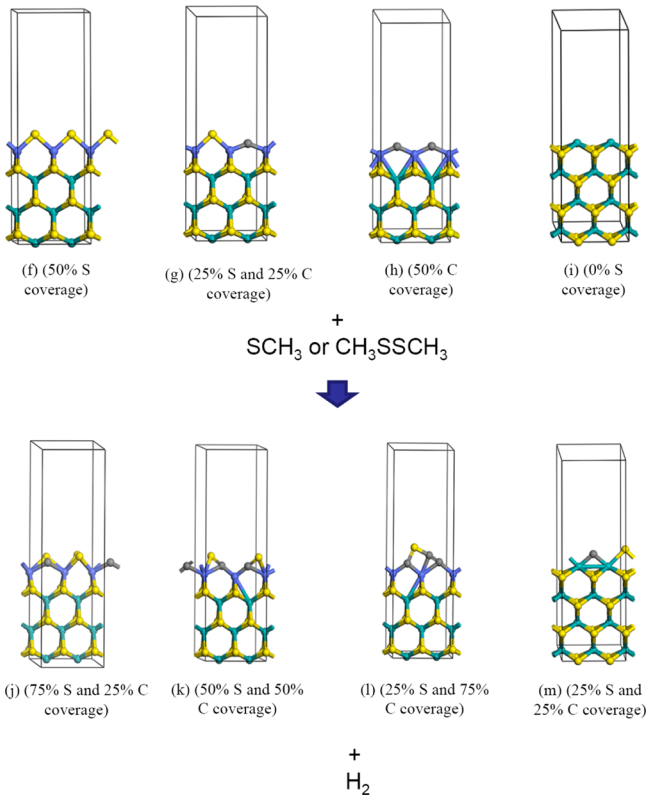

Figure 10. Simultaneous sulfidation and carburization by CH_3S or CH_3SSCH_3 on the S edge and the Mo edge.

Table 4. Relative Energy (ΔE, eV) of Simultaneous Sulfidation and Carburization by CH_3S or CH_3SSCH_3

process[a]	edge	from	to	CH_3S	CH_3SSCH_3
f to j	S	50% S	75% S and 25% C	1.53	2.88
g to k	S	25% S and 25% C	50% S and 50% C	−0.57	0.78
h to l	S	50% C	25% S and 75% C	−1.65	−0.30
i to m	Mo	0% S	25% S and 25% C	−1.02	0.32

[a]Process is schematized in Figure 10.

found that simultaneous carburization and sulfidation is only favored at sulfur edge with some carbon replacements, or at naked Mo edge. Due to cobalt promoter chelated by EN, the carburization of EN may take place at the surface of Co-promoter during sulfidation, leading to the establishment of the carbon unsaturated edge. And then it can serve as the surface for the simultaneous carburization and sulfidation by the organic sulfiding agent.

About the carbide-like structures, some questions still remain. For example, does the carbide carbon, like some authors proposed, have a positive effect on the hydrogenation and desulfurization of the sulfur containing molecules? Is it also stable at reactive conditions? Can it be formed through a process other than the addition of chelating agent? Elucidating these problems is the objective of the future research.

As for CoMo catalysts added with chelating agent and sulfided by organic sulfiding agent, the carbonizations by organic sulfiding agent, chelating agent (may include feed) will form different carbon species at different locations and with different effects. The carbon deposits as support make the interaction between active metals and support weakened and it improve the HDS activity. Coke-like carbon deposits cover the active sites, decreasing the HDS activity. The EN coordinating with Co^{2+} facilitates the formation of Co−Mo−S structures due to postponing the sulfidation of cobalt; but the carbonization of EN can retard the Co^{2+} access to the MoS_2 slabs. The carbide-like structures may be formed at the edges of active phase; but the actual effect on catalytic activity is unclear. Owing to the complexity of carbon species, the influences involving carbon species on HDS performance are also complicated. The contradictory results among literature may come from the difference of carbon species on the catalyst owing to the difference of catalyst preparation, sulfiding condition, reaction condition and feed, etc. How to effectively utilize the advantageous effects and suppress the adverse effects of carbonizations should be an important aspect of future HDS catalyst development.

4. CONCLUSION

We investigated the carbonization, sulfidation, and HDS of CoMo catalysts with addition of EN both experimentally and theoretically. The main results are summarized as follows:

(1) CoMo catalysts with addition of appropriate EN (Co:EN = 1) show enhanced sulfiding degree and improved thiophene HDS activities.

(2) EN coordinating with Co^{2+} postpones the sulfidation of cobalt. The sulfidation of molybdenum precedes that of cobalt. So the edges of MoS_2 slabs serve as anchoring sites for the Co promoters, and the addition of EN ligands avoids the formation of $CoAl_2O_4$ spinel. It is also favored for cobalt sulfidation. However, the carbonization of ligands can cover cobalt, resulting in the carbon packed Co_9S_8 particles. Therefore, the amount of EN should be controlled carefully.

(3) The carbide-like structures can be formed by two processes: Co-promoters at the edges of (Co)MoS_x are carburized by the coordinated EN molecules, and the active edge is simultaneously carburized and sulfided with DMDS as both carbon and sulfur source.

(4) Support-like carbon species located between (Co)MoS_x particle and alumina support reduce interaction between active metals and support, leading to a positive influence on the sulfidation and the final catalytic activity.

(5) Coke-like carbon deposits covering the surface of the active metals inhibit catalytic activity.

■ ASSOCIATED CONTENT

Supporting Information

Supplementary data and related discussion. This material is available free of charge via the Internet at http://pubs.acs.org.

■ AUTHOR INFORMATION

Corresponding Authors

*E-mail: gehui@sxicc.ac.cn.
*E-mail: wenxiaodong@gmail.com.
*E-mail: lxk@sxicc.ac.cn.

Notes

The authors declare no competing financial interest.

■ ACKNOWLEDGMENTS

The authors are grateful for the financial supports of the "Strategic Priority Research Program" Demonstration of Key Technologies for Clean and Efficient Utilization of Low-rank Coal (Grant No. XDA07020400). We acknowledged the Foundation of State Key Laboratory of Coal Conversion (Grant No. J13-14-301), the innovation foundation of Institute of Coal Chemistry, Chinese Academy of Sciences (No. Y4SC821981), Hundred People Plan of Chinese Academy of Sciences, and are grateful for Computer Network Information Center of Chinese Academy of Sciences providing Material Studio software and the Deepcomp7000 of Supercomputing Center, and we thank the Material Research and Technology Institute of University of Texas at El Paso.

■ REFERENCES

(1) Chianelli, R. R.; Berhault, G.; Torres, B. *Catal. Today* **2009**, *147*, 275−286.
(2) Wang, H.; Male, J.; Wang, Y. *ACS Catal.* **2013**, *3*, 1047−1070.
(3) Wivel, C.; Candia, R.; Clausen, B. S.; Mørup, S.; Topsøe, H. *J. Catal.* **1981**, *68*, 453−463.
(4) Derouane, E. G.; Pedersen, E.; Clausen, B. S.; Gabelica, Z.; Candia, R.; Topsøe, H. *J. Catal.* **1986**, *99*, 253−261.
(5) Daage, M.; Chianelli, R. R. *J. Catal.* **1994**, *149*, 414−427.
(6) Ramos, M.; Berhault, G.; Ferrer, D. A.; Torres, B.; Chianelli, R. R. *Catal. Sci. Technol.* **2012**, *2*, 164−178.
(7) Hallie, H. *Oil Gas J.* **1982**, *80*, 69−74.
(8) Kelty, S. P.; Berhault, G.; Chianelli, R. R. *Appl. Catal., A* **2007**, *322*, 9−15.
(9) Breyssea, M.; Afanasiev, P.; Geantet, C.; Vrinat, M. *Catal. Today* **2003**, *86*, 5−16.
(10) Berhault, G.; Cota, L.; Duarte, A.; Mehta, A.; Chianelli, R. R. *Catal. Lett.* **2002**, *78*, 81−90.
(11) Wen, X.-D.; Cao, Z.; Li, Y.-W.; Wang, J.; Jiao, H. *J. Phys. Chem. B* **2006**, *110*, 23860−23869.
(12) Tuxen, A.; Gøbel, H.; Hinnemann, B.; Li, Z.; Knudsen, K. G.; Topsøe, H.; Lauritsen, J. V.; Besenbacher, F. *J. Catal.* **2011**, *281*, 345−351.
(13) Yamada, S.; Qian, W.; Ishihara, A.; Wang, G.; Li, L.; Kabe, T. *Sekiyu Gakkaishi* **2001**, *44*, 217−224.
(14) Qian, W.; Yamada, S.; Ishihara, A.; Ichinoseki, M.; Kabe, T. *Sekiyu Gakkaishi* **2001**, *44*, 225−231.
(15) Texier, S.; Berhault, G.; Pérot, G.; Harlé, V.; Diehl, F. *J. Catal.* **2004**, *223*, 404−418.
(16) Texier, S.; Berhault, G.; Pérot, G.; Diehl, F. *Appl. Catal., A* **2005**, *293*, 105−119.
(17) Glasson, C.; Geantet, C.; Lacroix, M.; Labruyère, M.; Dufresne, P. *J. Catal.* **2002**, *212*, 76−85.
(18) Alonso, G.; Berhault, G.; Aguilar, A.; Collins, V.; Ornelas, C.; Fuentes, S.; Chianelli, R. R. *J. Catal.* **2002**, *208*, 359−369.
(19) Alvarez, L.; Espino, J.; Ornelas, C.; Rico, J. L.; Cortez, M. T.; Berhault, G.; Alonso, G. *J. Mol. Catal. A: Chem.* **2004**, *210*, 105−117.
(20) Ge, H.; Liang, F.; Li, X.; Qin, Z.; Wang, J. *Korean J. Chem. Eng.* **2009**, *26*, 576−581.
(21) Lélias, M. A.; Kooyman, P. J.; Mariey, L.; Oliviero, L.; Travert, A.; van Gestel, J.; van Veen, J. A. R.; Maugé, F. *J. Catal.* **2009**, *267*, 14−23.
(22) Lélias, M. A.; Le Guludec, E.; Mariey, L.; van Gestel, J.; Travert, A.; Oliviero, L.; Maugé, F. *Catal. Today* **2010**, *150*, 179−185.
(23) Rana, M. S.; Ramírez, J. R.; Gutiérrez-Alejandre, A.; Ancheyta, J.; Cedeño, L.; Maity, S. K. *J. Catal.* **2007**, *246*, 100−108.
(24) Sun, M.; Nicosia, D.; Prins, R. *Catal. Today* **2003**, *86*, 173−189.
(25) Pashigreva, H. V.; Bukhtiyarova, G. A.; Klimov, O. V.; Chesalov, Yu. A.; Noskov, G. S. *Catal. Today* **2010**, *149*, 19−27.
(26) Kishan, G.; Coulier, L.; van Veen, J. A. R.; Niemantsverdriet, J. W. *J. Catal.* **2001**, *200*, 194−196.
(27) Infantes-Molina, A.; Romero-Pérez, A.; Sánchez-González, V.; Pawelec, B.; Fierro, J. L. G.; Jiménez-López, A.; Rodríguez-Castellón, E. *ACS Catal.* **2011**, *1*, 175−186.
(28) Topsøe, H.; Clausen, B. S.; Massoth, F. E. In *Catalysis Science and Technology*; Anderson, J. R., Boudart, M., Eds.; Springer-Verlag: New York, 1996; Vol. *11*, p 31.
(29) Ge, H.; Li, X.; Fan, W.; Qin, Z.; Lü, Z.; Wang, J. *Chin. J. Catal.* **2009**, *30*, 111−118.
(30) Rueda, N.; Bacaud, R.; Vrinat, M. *J. Catal.* **1997**, *169*, 404−406.
(31) Cattaneo, R.; Shido, T.; Prins, R. *J. Catal.* **1999**, *185*, 199−212.
(32) Badoga, S.; Mouli, K. C.; Soni, K. K.; Dalai, A. K.; Adjaye, J. *Appl. Catal., B* **2012**, *125*, 67−84.
(33) Escobar, J.; Barrera, M. C.; Toledo, J. A.; Cortés-Jácome, M. A.; Angeles-Chávez, C.; Núñez, Sara; Santes, V.; Gómez, E.; Díaz, L.; Romero, E.; Pacheco, J. G. *Appl. Catal., B* **2009**, *88*, 564−575.
(34) Guichard, B.; Roy-Auberger, M.; Devers, E.; Pichon, C.; Legens, C. *Appl. Catal., A* **2009**, *367*, 1−8.
(35) Wen, X.-D.; Zeng, T.; Li, Y.-W.; Wang, J.; Jiao, H. *J. Phys. Chem. B* **2005**, *109*, 18491−18499.
(36) Ternan, M.; Furimsky, E.; Parsons, B. I. *Fuel Process. Technol.* **1979**, *2*, 45−55.
(37) Bogdanor, J. M.; Rase, H. F. *Ind. Eng. Chem. Prod. Res. Dev.* **1986**, *25*, 221−229.
(38) Koh, J. H.; Lee, J. J.; Kim, H.; Cho, A.; Moon, S. H. *Appl. Catal., B* **2009**, *86*, 176−181.
(39) Wen, X.-D.; Zeng, T.; Teng, B.-T.; Zhang, F.-Q.; Li, Y.-W.; Wang, J.; Jiao, H. *J. Mol. Catal. A: Chem.* **2006**, *249*, 191−200.
(40) Jacobsen, C. J. H.; Törnqvist, E.; Topsøe, H. *Catal. Lett.* **1999**, *63*, 179−183.
(41) Topsøe, H.; Hinnemann, B.; Nørskov, J. K.; Lauritsen, J. V.; Besenbacher, F.; Hansen, P. L.; Hytoft, G.; Egeberg, R. G.; Knudsen, K. G. *Catal. Today* **2005**, *107−108*, 12−22.
(42) Papadopoulou, Ch.; Vakros, J.; Matralis, H. K.; Voyiatzis, G. A.; Kordulis, Ch. *J. Colloid Interface Sci.* **2004**, *274*, 159−166.
(43) Ramos, M.; Ferrer, D.; Martinez-Soto, E.; Lopez-Lippmann, H.; Torres, B.; Berhault, G.; Chianelli, R. R. *Ultramicroscopy* **2013**, *127*, 64.
(44) Hayden, T. F.; Dumesic, J. A.; Sherwood, R. D.; Baker, R. T. K. *J. Catal.* **1987**, *105*, 299−318.
(45) Candia, R.; Sørensen, O.; Villadsen, J.; Topsøe, N.-Y.; Clausen, B. S.; Topsøe, H. *Bull. Soc. Chim. Belg.* **1984**, *93*, 763−773.
(46) Topsøe, N.-Y.; Topsøe, H. *J. Catal.* **1993**, *139*, 631−640.
(47) van Veen, J. A. R.; Hendriks, P. A. J. M.; Romers, E. J. G. M.; Andréa, R. R. *J. Phys. Chem.* **1990**, *94*, 5275−5282.
(48) Joshi, Y. V.; Ghosh, P.; Daage, M.; Delgass, W. N. *J. Catal.* **2008**, *257*, 71−80.
(49) Lauritsen, J. V.; Kibsgaard, J.; Olesen, G. H.; Moses, P. G.; Hinnemann, B.; Helvegc, S.; Nørskov, J. K.; Clausen, B. S.; Topsøe, H.; Lægsgaard, E.; Besenbacher, F. *J. Catal.* **2007**, *249*, 220−233.
(50) Krebs, E.; Silvi, B.; Raybaud, P. *Catal. Today* **2008**, *130*, 160−169.